Efficacy of a portable, moderate-resolution, fast-scanning DMA for ambient aerosol size distribution measurements

Stavros Amanatidis[1,2], Yuanlong Huang[1], Buddhi Pushpawela[1], Benjamin C. Schulze[1], Christopher M. Kenseth[1], Ryan X. Ward[1], John H. Seinfeld[1], Susanne V. Hering[2], and Richard C. Flagan[1,*]

[1]California Institute of Technology, Pasadena, CA, USA
[2]Aerosol Dynamics Inc., Berkeley, CA, USA

Correspondence: Richard C. Flagan (flagan@caltech.edu)

Abstract.

Ambient aerosol size distributions obtained with a compact, scanning mobility analyzer, the "Spider" DMA, are compared to those obtained with a conventional mobility analyzer, with specific attention to the effect of mobility resolution on the measured size distribution parameters. The Spider is a 12-cm diameter radial differential mobility analyzer that spans the 10–500 nm size range with 30 s mobility scans. It achieves its compact size by operating at a nominal mobility resolution $R = 3$ (sheath flow = 0.9 L/min, aerosol flow = 0.3 L/min), in place of the higher sheath-to-aerosol flow commonly used. The question addressed here is whether the lower resolution is sufficient to capture ~~the dynamics and~~ key characteristics of ambient aerosol size distributions. The Spider, operated at $R = 3$ with 30 s up and down scans, was collocated with a TSI 3081 long-column mobility analyzer, operated at $R = 10$ with a 360 s sampling duty cycle. Ambient aerosol data were collected over 26 consecutive days of continuous operation, in Pasadena, CA. Over the 17~~20~~–500 nm size range, the two instruments exhibit excellent correlation in the total particle number concentrations and geometric mean diameters, with regression slopes of 1.13 and 1.00, respectively. Our results suggest that particle sizing at a lower resolution than typically employed may be~~is~~ sufficient to obtain~~in obtaining~~ key properties of ambient size distributions, at least for these two moments of the size distribution. Moreover, it enables better counting statistics, as the wider transfer function for a given aerosol flowrate results in a higher counting rate.

1 Introduction

Mobility measurements of atmospheric aerosols in the 10–500 nm size range are important to atmospheric aerosol characterization (McMurry, 2000). Measurements aloft are especially important to understand aerosols in remote regions (Creamean et al., 2020; Herenz et al., 2018), and to mapping three-dimensional profiles (Mamali et al., 2018; Ortega et al., 2019; Zheng et al., 2021). Traditional mobility analyzers that span this size range are large~~,~~ and not suitable for most unmanned aerial vehicle (UAV) or tethered balloon payloads, which~~that~~ increasingly serve as ~~the~~ platforms for aerosol characterization aloft. Moreover, aircraft measurements also require a fast scan time resolution to enable a good spatial resolution, as time is proportional to distance traveled in a moving platform.

To that end, Amanatidis et al. (2020) developed the "Spider DMA", a compact, lightweight, and fast differential mobility analyzer (DMA). The instrument was designed for 10–500 nm sizing, with an aerosol flowrate of 0.3 L/min to provide adequate counting statistics on ambient aerosol over the time window appropriate for moving platforms. Its~~However, its~~ compact size was achieved in part through reduction of mobility resolution. I~~; i~~nstead of the typical ~~factor of 10~~ ratio of sheath-to-aerosol flows of 10 ~~between the sheath and aerosol flows~~, the Spider DMA employs a flow ratio~~factor~~ of 3. For given sample flowrate, the most commonly used flowrate ratio of 10 requires a larger sheath flow, which in turn requires a larger mobility analyzer to reach the same maximum particle size.~~obtaining higher resolution requires increasing the sheath flowrate, which in turn comes at the expense of dynamic sizing range; thus, a larger classifier would be required to maintain both sizing range and high resolution.~~

While high size resolution is important for specific applications, such as in laboratory calibrations that employ a DMA as a calibration aerosol source, it may not be critical for ambient size distribution measurements, wherein the particle distribution spans a much wider size range than the transfer function of the DMA. Lower DMA resolution has also been successfully employed for reconstructing aerosol dynamics process rates in chamber experiments (Ozon et al., 2021). In addition to the smaller physical size ~~for~~of the instrument, operating at lower resolution increases the particle count rate owing to the wider DMA mobility window, thereby reducing measurement uncertainty.~~results in higher number of particle counts per size bin, and thus decreases the statistical uncertainty.~~ This can be an important factor for low-concentration measurements. Moreover, the resulting lower sheath flow requirements enable the usage of more compact and less power-demanding pumps, which further facilitates the overall portability of the instrument.

The question explored in this paper is whether the moderate resolution mobility sizing of the Spider DMA is sufficient to capture the important characteristics of atmospheric aerosol size distributions. We begin with the derivation of the Spider DMA transfer function through a combination of finite element simulations and laboratory calibrations. We then present a field validation by comparison of ambient aerosol data from the new instrument with that obtained from a traditional long-column cylindrical DMA (LDMA) operated at a nominal resolution of $R = 10$ during nearly one month of continuous operation of the two, co-located instruments.

2 Methods

2.1 Spider DMA

The prototype Spider DMA sizing system consists of the "Spider" DMA (Amanatidis et al., 2020) and the "MAGIC" particle counter (Hering et al., 2014, 2019). The Spider is a compact mobility analyzer designed for applications requiring high portability and time resolution. It features a radial flow geometry and a sample inlet ~~distribution~~ system that distributes~~where~~ the flow ~~is~~ azimuthally ~~distributed~~ through curved ("Spider"-like) flow channels. The instrument was designed to operate at 0.3 L/min sample and 0.6–1.2 L/min sheath flowrates, offering size classification in the 10–500 nm size range. Owing to its small classification volume, the mean gas residence time in the classifier is on the order of ~ 1 s, making it possible to complete its voltage scan in times well below 60 s without significant smearing of its transfer function.

The "MAGIC" (Moderated Aerosol Growth with Internal water Cycling) particle counter is a laminar-flow water-based CPC. It employs a particle growth tube chamber with three stages (cool, warm, and cool) in which ultrafine particles grow by heterogeneous water vapor condensation to $> 1\,\mu\mathrm{m}$, and are subsequently counted by an optical detector. The final stage of the MAGIC CPC growth tube (moderator) recovers excess water vapor, enabling long-term operation without the need of a reservoir or water refilling. The instrument operates at a sample flowrate of 0.3 L/min, and has a 50% detection cut-point of $\sim$ 67 ~~7~~ nm.

2.2 Transfer function determination by finite element modeling

Amanatidis et al. (2020) evaluated the Spider DMA transfer function in static-mode based on the Stolzenburg (1988) transfer function model and its derivation for radial flow classifiers (Zhang et al., 1995; Zhang and Flagan, 1996). Here, we evaluate its transfer function in ~~at~~ "scanning" mobility mode, wherein the electric field is varied continuously in an exponential voltage ramp (Wang and Flagan, 1990). The scanning transfer function was evaluated with 2D finite element COMSOL Multiphysics simulations of flows, quasi-steady-state electric field, and particle trajectories~~, using COMSOL Multiphysics~~. Simulations were performed for 0.9 L/min sheath and 0.3 L/min aerosol ~~0.9/0.3 L/min sheath /aerosol~~ flowrates, scanning voltage in the range 5 – 5000 V, and 30 s exponential ramps for both up- and down-scans. Particles were modeled with the "Mathematical particle tracing" module, in which particle mass was assumed to be negligible since the electric field varies slowly, on a time scale that is long compared to the aerodynamic relaxation time of the particles being measured. Particle trajectories ~~motion was~~ were calculated ~~explicitly,~~ by assigning particle velocity vector components equal to the steady-state fluid field solution, combined with the axial velocity acquired from interaction with the time-varying electrostatic field. Moreover, a Gaussian random-walk was employed in each time step of the solver to simulate particle Brownian motion, with a standard deviation proportional to particle diffusivity, i.e. $\mathrm{d}\sigma = \sqrt{2\,D\,\mathrm{d}t}$. Monodisperse particles were injected in regular intervals over the scan, varying from 0.025 s for large particles to 0.003 s for those in the diffusing size range to capture in sufficient detail the Brownian motion along the particle trajectories. Modeling was repeated for 10 discrete particle sizes, spanning the dynamic range of the classifier. Details on the Spider DMA geometry employed in the modeling, as well as an example with particle trajectories over the Spider voltage scan are included in the supplementary material (Figures S1 and S2).

2.3 Experimental

The two sizing instruments, the Spider DMA and the LDMA system, were operated in parallel, sampling ambient air from a roof top at the Caltech campus in Pasadena, CA. Measurements were made between May 16 – June 11, 2020, and were done as part of a study of the impacts of the COVID-19 pandemic shut-down on air quality. The experimental setup used is shown in Figure 1. Ambient aerosol samples passed through a soft X-ray charge conditioner, and were subsequently split between the two mobility sizing systems, thereby ensuring that the charge status of the aerosols seen by the two instruments was identical. The charge conditioner is a prototype device that was developed recently at Caltech. It is based upon a Hamamatsu soft X-ray source that directly ionizes the air around the incoming aerosol flow. Both DMA systems were operated in scanning mode.

Both used a MAGIC water-based CPC as the detector. The size pre-cut stage in the inlet of both CPCs was removed to avoid additional smearing of the transfer functions.

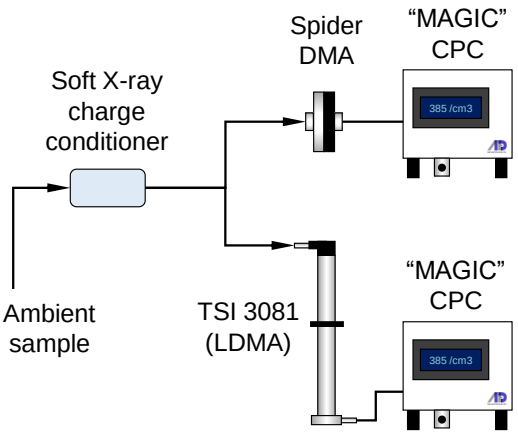

Figure 1. Schematic of the experimental setup used to evaluate the Spider DMA. The prototype instrument was operated at 0.9 L/min sheath and 0.3 L/min aerosol flowrates, and a scanning voltage program consisting of a 30 s upscan followed by a 30 s downscan. A TSI 3081 long-column DMA, operated at 3.0 L/min sheath and 0.3 L/min aerosol flows, 240 ~~330~~s upscans, was used for comparison. Both sizing systems used an ADI "MAGIC" CPC as the particle detector.

The Spider DMA was operated at 0.9 L/min sheath and 0.3 L/min aerosol flowrates. A piezoelectric blower (Murata, MZB1001T02) was enclosed into a sealed housing to serve as a recirculating pump for the Spider sheath flow. The pump assembly weighs ~ 60 g. Operating at a frequency of 24-27 kHz, this pump produces only very small pressure fluctuations that are effectively damped by the capacitance of the downstream filter. With feedback control, the pump attains a steady flow up to ~ 1 L/min within about 1 s, making it well suited to operating in an environment in which the pressure varies slowly, as in UAV applications. The Spider DMA scanning program included a 30 s upscan followed by a 30 s downscan, during which the electrode voltage was exponentially varied between 5 – 5,000 V. The voltage was held steady for an additional 2 s at each end of the voltage ramp to allow for incoming particles to transmit through the classifier. Particle counts over the scan were recorded with a 5 Hz rate.

The LDMA system was based on a TSI 3081 long-column DMA operated at 3.0 L/min sheath and 0.3 L/min aerosol flowrates, offering classification in the 17–989 nm size range. The scans consisted of an exponentially increasing (upscan) voltage ramp between 25–9,875 V with a 240 ~~330~~s duration. As with the Spider DMA, the LDMA voltage was held constant at the beginning and end of the ramp ~~for 15s~~. Owing to its longer mean flow residence time, the LDMA voltage hold periods were set at 40 s, bringing its overall duty cycle to 360 s. Particle counts for the LDMA system were recorded with a 2 Hz sampling rate. Data acquisition and instrument control (flows, high voltage) was performed with custom LabVIEW software for both systems.

2.4 DMA scanning conditions

Comparison of the scanning voltage conditions between the two DMAs requires accounting for differences in geometry, flowrates, and voltage scanning rates. The appropriate non-dimensional quantity that describes the DMA scanning rate is given by $\theta_s = \frac{\tau_{HV}}{t_g}$, the ratio of the exponential voltage ramp time constant, τ_{HV}, to the classifier mean gas residence time, t_g. At large θ_s values, typically $\theta_s > 10$, the rate at which the scanning voltage varies as particles transmit through the classifier is slow, and the transfer function approximates the "static" DMA transfer function. At small θ_s values, the scanning voltage changes quickly relative to the particle residence time, smearing the transfer function, which becomes pronounced as θ_s approaches unity (Russell et al., 1995; Collins et al., 2004). For the Spider DMA operating conditions, $\tau_{HV} = 4.34$ s and $t_g = 1.30$ s, resulting in $\theta_s = 3.35$. For the LDMA, $\tau_{HV} = 40.14$ s and $t_g = 7.52$ s, resulting in $\theta_s = 5.34$. Here, even though τ_{HV} of the LDMA is about 10 times larger (i.e., slower) than that of the Spider, its dimensionless scanning rate (θ_s) is only about 1.6 times smaller owing to its much longer flow residence time. In absolute terms, the scanning rate employed in both DMAs is moderate.

2.5 Data inversion & analysis

Particle size distributions were obtained by inverting the raw particle counts recorded over each voltage scan. Raw counts were smoothed prior the inversion to minimize inversion artifacts. ~~by~~ Locally Weighted Scatterplot Smoothing (LOWESS) regression (Cleveland, 1979) was employed for the Spider DMA data with a 10% smoothing window (i.e., 15 data points). The LDMA raw counts were smoothed by applying a moving average filter with a span of 5 data points. The smoothed data were then inverted by ~~employing~~ regularized non-negative least squares minimization ~~for both systems~~. Tikhonov regularization was used for both systems, with $\lambda = 0.140$ and $\lambda = 0.015$ regularization parameters for the Spider DMA and LDMA data, respectively. Those values were found to provide stable solutions without over-constraining the inversion results.

The inversion kernel for the Spider DMA system was based on the scanning transfer function of the Spider DMA obtained by finite element modeling. In order to generate a dense kernel required for the inversion, the modeled transfer function data were fitted to~~in~~ Gaussian distributions, whose parameters were subsequently fitted to analytical expressions that allowed generation of transfer functions at any instant (i.e., time bin) over the voltage scan. The Spider transfer functions were subsequently convoluted with a continuous stirred-tank reactor (CSTR) model (Russell et al., 1995; Collins et al., 2002; Mai et al., 2018) to take into account the time response of the MAGIC CPC. A 0.35 s time-constant was used for the CSTR model in the Spider DMA system (Hering et al., 2017). The resulting transfer function was combined with a size-dependent transmission efficiency model described by Amanatidis et al. (2020) to take into account particle losses occurring at the Spider inlet, as those are not evaluated in the 2D finite element modeling. Raw counts were shifted to earlier time bins to account for the 1.50 s plumbing time delay between the Spider outlet and the MAGIC CPC detector. Because the simulation enabled a strictly monodisperse "calibration" aerosol, the ratio of the number exiting the DMA during a particular counting time interval to~~over~~ the upstream particle number is the instrument transfer function. The kernel for the LDMA system was based on the scanning transfer function model derived recently by Huang et al. (2020). A CSTR model with a characteristic time of 0.35 s, and a plumbing

delay time of 0.95 s were used to incorporate the response of the MAGIC CPC used in the LDMA system. ~~The particle charge probability in the data inversion for both systems was assumed to follow the Wiedensohler approximation of the Boltzmann charge distribution (Wiedensohler, 1988).~~

The Wiedensohler (1988) fit to the Hoppel and Frick (1986) numerical evaluation of the Fuchs (1963) charge distribution has been used in the data inversion. Note that, since both instruments sampled from the same soft X-ray charge conditioner, any deviations from the assumed charge distribution will not affect the comparison between the two instruments.

3 Results

3.1 Spider scanning transfer function

Figure 2 shows the scanning transfer function of the Spider DMA evaluated by finite element modeling. Results are plotted as a function of time in the scan, for upscan and downscan voltage ramps. Each peak represents the ratio of particle number at the outlet to~~over~~ the inlet, for a specific input particle size. Finite element modeling data, shown with symbols, have been fitted to Gaussian distributions, shown with solid lines, which provide a close approximation to both upscan and downscan modeling data. As will be shown next, the Gaussian fits are subsequently employed to generate the transfer function at any time instance over the scan.

Comparison between upscan and downscan peaks reveals a distinct difference; downscan peaks have a higher maximum number ratio. Moreover, they are somewhat narrower than the upscan peaks. It should be noted that the transmission efficiency through the classification zone of a DMA is proportional to the area under the peak, rather than its maximum value. Hence, particle transmission over downscans is not necessarily higher than upscans. Here, the area of the Gaussian curves used to fit the transfer function modeling data was on average ~3.5% larger for downscans than upscans. This difference is likely due to the slightly asymmetrical shape of the downscan transfer function, which can be observed at the onset (i.e., lower left side) of each peak in Figure 2b where the fitted curves are somewhat wider than the modeling data. A closer comparison between upscan and downscan fitting parameters is provided in the supplementary material (Figure S3). Diffusional broadening of the transfer function becomes important in the low voltage region of each ramp, increasing the transfer function width as voltage decreases, though the broadening is less than would be seen with a higher resolution DMA (Flagan, 1999).

The differences in the transfer function between upscans and downscans is the result of the scanning voltage operating mode and particle interaction with the boundary flow layers near the DMA electrode walls. Owing to the laminar flow profile, particles near the electrode walls acquire lower velocities than those in middle of the electrode gap. Over downscans, a fraction of the incoming particles interacts with the boundary layer adjacent to the wall that houses the exit slit of the classifier. As voltage drops below a certain threshold, those particles reach the exit of the classifier, albeit with a time delay relative to particles of the same mobility whose trajectories did not interact with the boundary layer. This results in a particle exit time reallocation, which alters the shape of the downscan transfer function as the voltage drop becomes more rapid. This condition is inhibited over upscans, since the respective boundary layer is formed on the wall opposite to the exit flow, and is exhausted through the excess flow. Collins et al. (2004) and Mamakos et al. (2008) demonstrated the impact of scanning voltage on the transfer function of

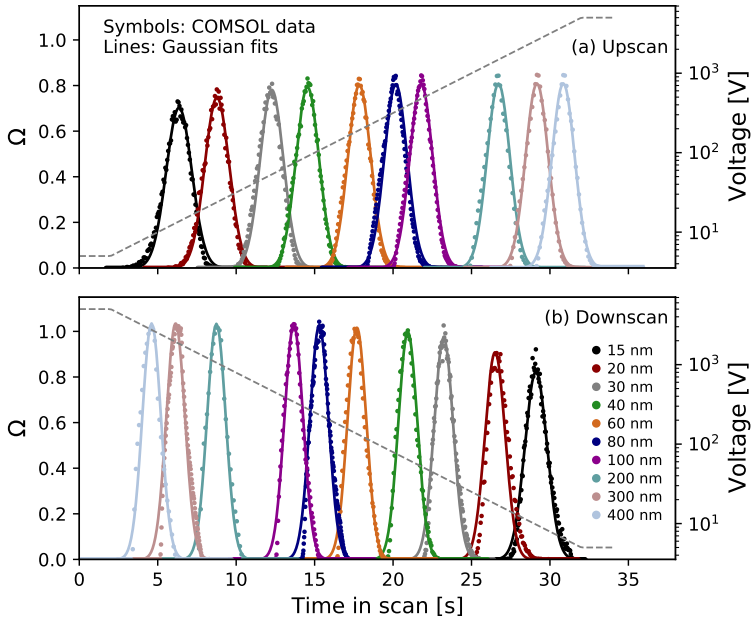

Figure 2. Finite element modeling of the Spider DMA scanning transfer function for (a) upscan and (b) downscan exponential voltage ramps with 30 s duration, 0.9 L/min sheath and 0.3 L/min aerosol flowrates. Symbols correspond to finite element modeling data (ratio of particle number at the outlet to~~over~~ the inlet); solid lines show Gaussian distributions fitted to the modeling data; dashed lines indicate the scanning voltage program (values shown on right y-axis).

the cylindrical DMA. Over downscans, the transfer function deviates from the symmetric triangular or Gaussian shape, and becomes skewed. The effect becomes larger for fast scans, and is significant when the effective scan rate $\theta_s < 2$. This is also true for the Spider DMA, as shown in Figure 2b, however the shape distortion is relatively small given the moderate Spider scan rate ($\theta_s = 3.4$). Moreover, in contrast to the cylindrical DMA, the boundary layers in the radial DMA are symmetric, which reduces the downscan distortion compared to its cylindrical counterpart. Over upscans, the width of the scanning transfer function broadens, but retains its symmetric shape. For this reason, downscan data are often discarded in scanning DMA data analyses, as the more irregular shape of the transfer function is more difficult to parameterize. However, this strategy comes with a penalty in sampling time resolution, owing to the "dead" time associated with the discarded downscan that is required after each upscan. The dead time required depends on the classifier mean gas residence time (typically > 2–$3 \times t_g$) and the capacitance of the DMA high-voltage supply. As the Spider DMA scanning transfer function can be described with good fidelity for both upscans and downscans, both are included in the data analysis to maximize its time resolution.

Figure 3 shows the integrated transfer function of the Spider DMA system for the same operating conditions as those used in the experiments. The voltage program, shown in Figure 3a, consists of a 2 s hold time at 5 V, followed by a 30 s upscan up to 5000 V, a 2 s hold time at 5000 V, and a 30 s downscan to 5 V. The classified particle size follows roughly the exponential increase and decrease of the voltage over the scan. The peaks shown in Figure 3b consist of the Gaussian approximation

of the Spider transfer function shown in Figure 2, combined with the size and time response of the MAGIC CPC, and the size-dependent transmission efficiency in the Spider inlet (Amanatidis et al., 2020).

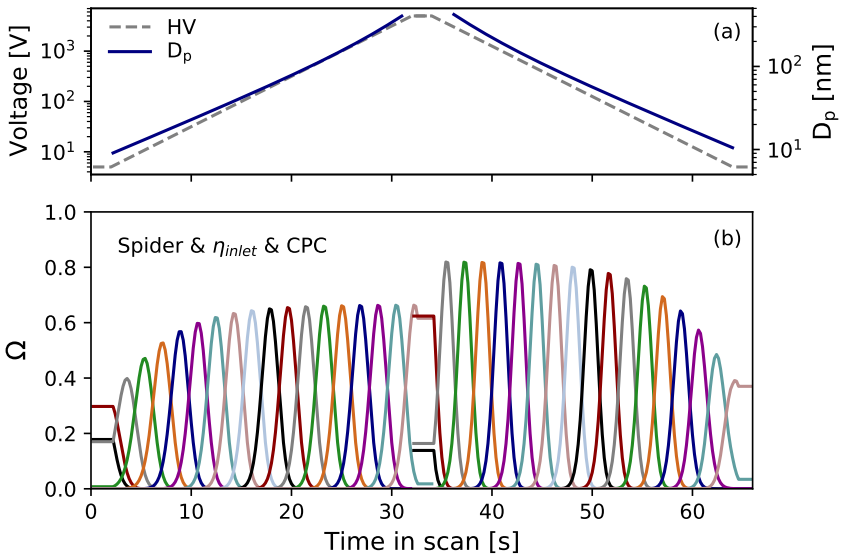

Figure 3. a) Scanning voltage and classified particle size over the Spider DMA scan. b) Transfer function of the integrated Spider DMA - MAGIC CPC system (ratio of particle number at the outlet toover the inlet), consisting of the Spider DMA scanning transfer function combined with its inlet transmission efficiency and the MAGIC CPC response.

3.2 Data inversion example

Figure 4 demonstrates an inversion example for representative Spider DMA data. Particle raw counts recorded at each time bin over the upscan and downscan are shown in Figure 4a. Smooth curveslines are fitted to the raw counts data to minimize artiefacts in the inversion process. The resulting size distributions, employing an inversion kernel based on the scanning transfer function in Figure 3b, are shown in Figure 4b. Up- and downscan distributions are almost identical in both shape and magnitude. The mean of the two distributions, as shown here, is used as the output of each scan. Overall, considering all measurement data collected in this work, upscan raw counts data inversion yielded distributions with consistent, but slightly higher ($3.7\% \pm 2.3\%$) total particle number than downscans.

3.3 Instrument comparison

Figure 5 demonstrates the effect of sizing resolution on the counting rate of the downstream particle detector. As both the Spider DMA and the LDMA operated at the same aerosol flowrate, one would expect a higher counting rate for the Spider DMA system owing to its wider transfer function. Indeed, as shown in Figure 5, this was the case. The data presented here are the average of particle count rates during upscans over an eighteen minute period (corresponding to 3 LDMA upscans, 17

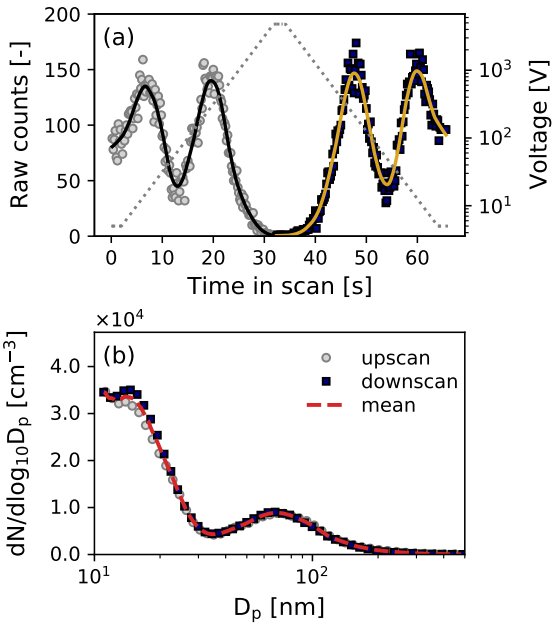

Figure 4. Example of Spider DMA data inversion. a) Raw counts per time bin (symbols) recorded over the voltage ramp (up- and downscan). Solid lines indicate LOWESS smoothing to the raw counts. b) Resulting size distributions after data inversion. The dashed line shows the mean of the up- and downscan distributions.

Spider upscans). This example was selected as a representative comparison case since the resulting particle counts distribution is centered near the middle of the overlapping mobility range. The integral of the counting rate with respect to scanning mobility for each instrument (i.e., area below the data points in Figure 5), was larger by a factor of 3.325 in the Spider measurement than the LDMA; this is almost exactly the same as the inverse of the sizing resolution ratio (i.e., 10 / 3) of the two DMAs. In fact, this ratio was rather consistent (within ±10%) despite the size distribution variation over the course of the day, corroborating that, for given aerosol flowrate, lower DMA resolution results in higher counting rates, thus enables better counting statistics.

Figure 6 illustrates an excerpt of the Spider and LDMA size distribution measurements over a time period of 3 days. The two instruments report similar diurnal variation in the particle size distribution, in both size and number concentration. Increased particle concentrations were recorded in the early afternoon of each day, a regular occurrence as particles from morning traffic are transported by the sea breeze from Los Angeles to Pasadena where the measurements took place. Concentrations begin to drop later in the afternoon and through the evening, from about 15,000 cm^{-3} to below 5,000 cm^{-3}. The geometric mean diameter (GMD) of the size distribution ranged between about 30–60 nm, and was smaller over the high number concentration events recorded in early afternoon.

Figure 7 shows the evolution of the size distribution over a period of 2 hours in the afternoon of May 28, 2020 (indicated with dashed box in Figure 6d), measured with the Spider and the LDMA system. Since the measurement duty cycle of the two instruments was different (66 s for the Spider vs 360 s for the LDMA), we employed 30 min averaging of the recorded size

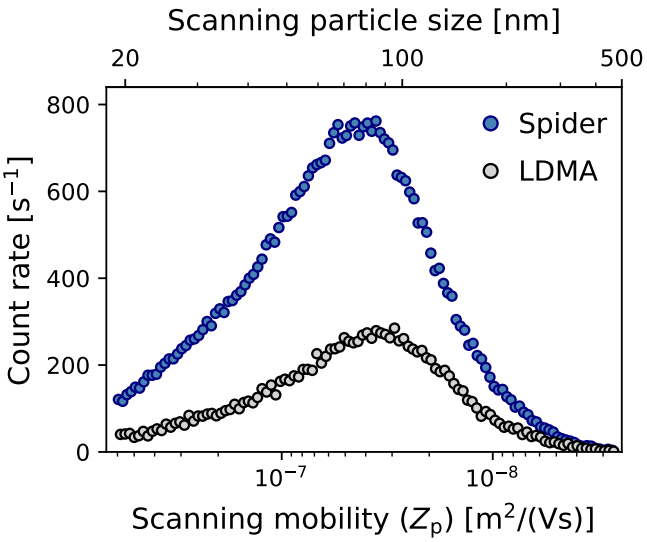

Figure 5. Sizing resolution effect on the particle count rate of the Spider DMA (R=3) and LDMA (R=10) systems. Data shown are the average of raw particle count rates during upscans over an eighteen minute period (corresponding to 3 LDMA upscans, 17 Spider upscans) measured in the morning of June 1, 2020. Both systems operated at 0.3 L/min aerosol flowrate.

distributions. This corresponds to 5 scans for the LDMA, and about 27 up- and down-scans for the Spider. The shaded areas of the averaged distributions represent the variation over the averaging period. Starting from a mono-modal distribution with a peak at ~ 45 nm (panel a), the size distribution transitioned to a bi-modal one over a period of 60 min (panels b, c), before transitioning back to a mono-modal distribution (panel d). As indicated by the shaded areas, there was high variation in the aerosol concentration during this transition event. Overall, the measurement of the two instruments was in good agreement both in terms of sizing and concentration, suggesting that the lower sizing resolution in the Spider DMA was adequate in capturing the details of the size distribution. An animation video with side-by-side comparison of 30-min averaged distributions for the entire testing period is included in the Supplementary Material (Amanatidis et al., 2021).

Figure 8 compares the total number and geometric mean diameter measured by the two instruments over the entire testing period. Each data point corresponds to a 1-hour average of the size distribution measured by each instrument, calculated over the 17–500 nm size range where the two systems overlap. Overall, the comparison includes 550 h of measurement data. In order to identify outliers in the data, we employed the "RANSCAC" (random sample consensus) algorithm (Fischler and Bolles, 1981). In this, random samples of the data are selected, analyzed, and classified as inliers and outliers through an iterative routine. The outliers identified are shown in Figure 8 with open square symbols.

Next, a linear regression model (no intercept) was fitted to the data (excluding outliers) to evaluate the correlation between the two instruments. Since both instruments include measurement errors, we employed Orthogonal Distance Regression (Boggs et al., 1987), where errors on both the dependent and independent variable are taken into account in the least squares minimiza-

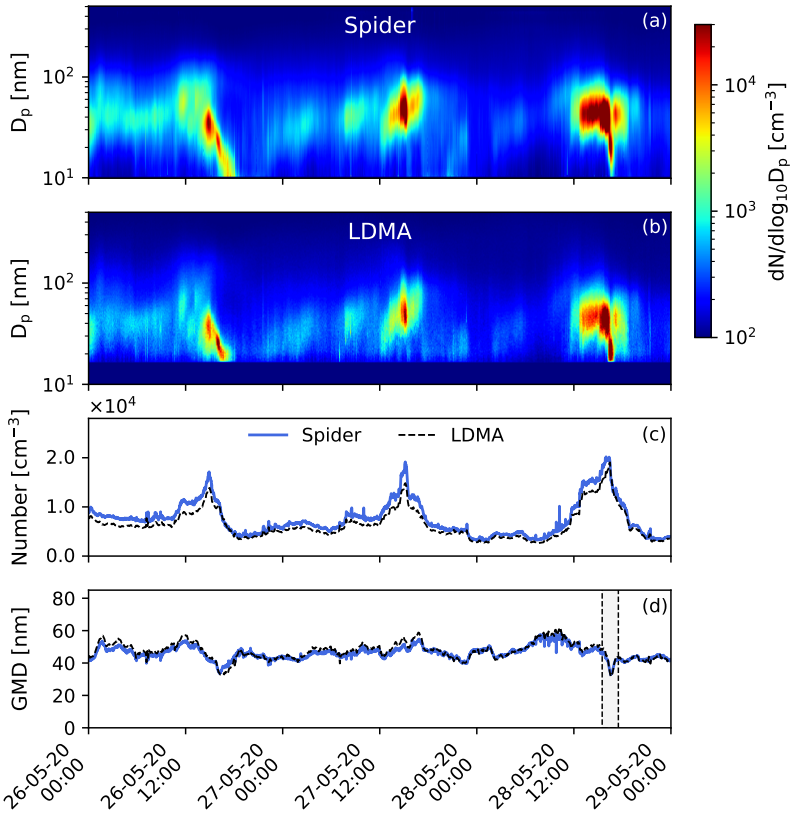

Figure 6. Evolution of the particle size distribution over a period of 3 days measured by a) the Spider DMA, and b) the LDMA system. Corresponding total particle number and geometric mean diameter, calculated over the 17–500 nm size range, are shown in panels (c) and (d), respectively. Solid blue color in panel (b) (size range <17 nm) was used for no available data in the LDMA system. The dashed box in panel (d) indicates the time period shown in Figure 7.

tion. The resulting regression lines exhibit slopes of $\alpha = 1.13$ and $\alpha = 1.00$ for number concentration and GMD, respectively, suggesting an overall excellent agreement between the instruments. Moreover, Pearson correlation coefficients of $\rho = 0.98$ and $\rho = 0.93$ indicate a strong correlation for both metrics of the size distribution.

3.4 Operational observations

240 The prototype Spider DMA used in this study incorporated an electrostatic-dissipative plastic that failed after several months of continuous operation, causing arcing within the instrument at the highest voltages. The Spider DMA has been redesigned to eliminate this material, and is currently being tested. This new Spider DMA has relatively minor changes to the classification region of the prototype presented here, and employs the same moderate resolution approach to maintain a compact size.

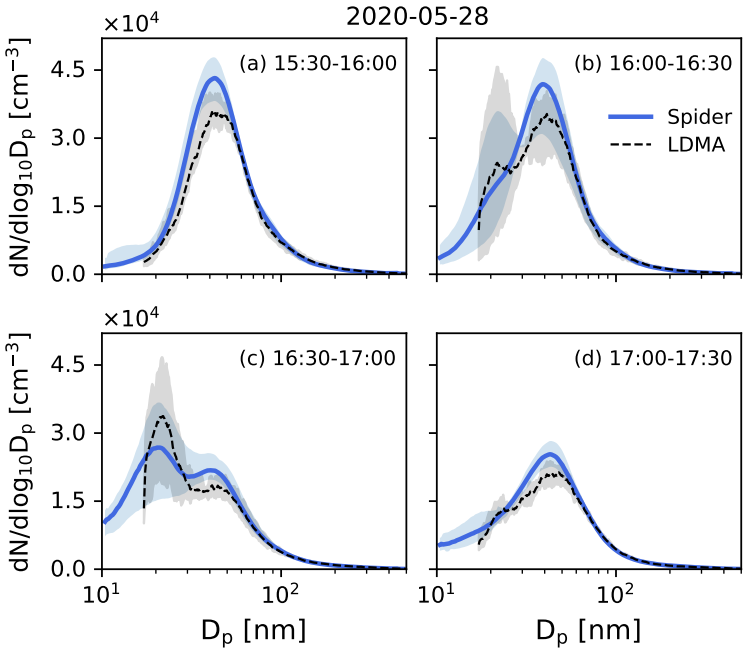

Figure 7. Evolution of the size distribution in the afternoon of May 28, 2020, as measured by the Spider and LDMA systems. Lines represent the mean of size distributions measured over a period of 30 min. Shaded areas demonstrate the variation of the size distribution over the averaging period, indicating maximum and minimum values.

4 Summary & conclusions

We evaluated the performance of the Spider DMA, a highly-portable particle sizer, in measuring ambient size distributions against a co-located particle sizer based on a TSI 3081 long-column DMA (LDMA). Comparison measurements were performed at the Caltech campus in Pasadena, CA over a period of 26 days, between May 16 – June 11, 2020, as part of a field campaign examining the effects of COVID-19 shut-down on air quality. The Spider DMA system was operated at a lower nominal sizing resolution (0.9 L/min sheath and 0.3 L/min aerosol flowrates, $R = 3$) than the LDMA (3.0 L/min sheath and 0.3 L/min aerosol flowrates, $R = 10$), and at a higher time resolution (30 s vs 240 s scans).

The transfer function of the Spider DMA was obtained by finite element modeling at the conditions employed in the experiment, which included both up- and downscan exponential voltage ramps with 30 s duration. Owing to the Spider radial flow geometry and short gas flow residence time, distortion of the downscan transfer function shape is minimal at the scan rates employed, enabling usage of both upscan and downscan data, thereby increasing time resolution. Modeling data were fitted to Gaussian distributions, and were combined with the experimentally-determined transmission efficiency of the Spider DMA and the MAGIC particle counter response function to generate the inversion kernel of the combined system. Data inversion of the LDMA system was based on the semi-analytical model of the LDMA scanning transfer function derived by Huang et al.

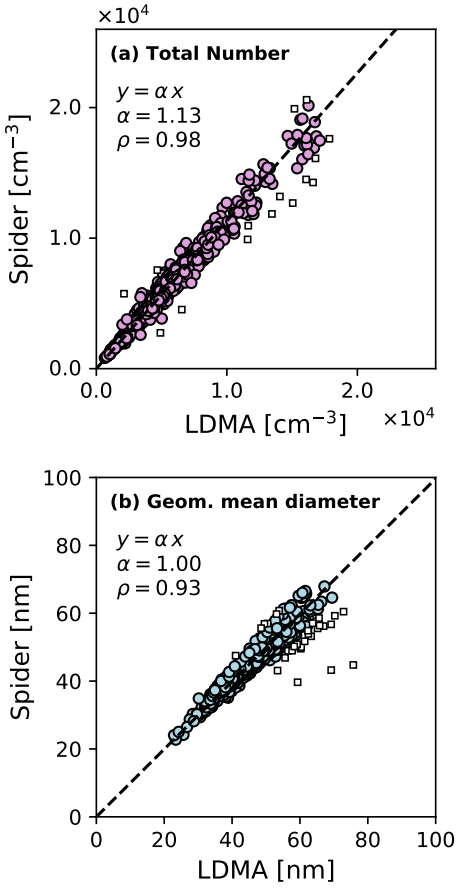

Figure 8. Comparison of a) total particle number, and b) geometric mean diameter, measured by the Spider and LDMA systems over a period of 26 days of continuous testing. Each point represents 1 hour averaged data, calculated over the 17–500 nm size range where the two instruments overlap. Square symbols show outliers excluded from the regression analysis. Dashed lines represent a linear regression model (no intercept) fitted to the data. ρ values denote the Pearson correlation coefficient between the measurement data of the two instruments.

(2020).

Regression analysis of 550 h of measurement data showed an overall excellent correlation between the two instruments, with slopes of $\alpha = 1.13$ and $\alpha = 1.00$, and Pearson correlation coefficients of $\rho = 0.98$ and $\rho = 0.93$ in the reported particle number and geometric mean diameter (GMD), respectively. ~~The good agreement between the two instruments suggests that particle sizers operated at moderate resolution ($R = 3$ in this study) can sufficiently capture the dynamics and key characteristics of ambient size distributions, at least in the 10–500 nm size range. Lowering the resolution enables a wider dynamic range, or a more compact particle sizer for a desired size range, which is essential in many field applications, such as for measurements aloft with small UAVs or tethered balloons that have limited payloads. Moreover, it enables better counting statistics, as the wider transfer function results in higher counts per size bin, which is an important factor at low concentration aerosol~~

~~measurements.~~ The present results suggest that two key characteristics of ambient size distributions, geometric mean diameter and number concentration, are sufficiently captured when operating the DMA at lower resolution than is typically employed. Moreover, use of lower resolution, where appropriate, has several distinct advantages. For the same aerosol flow rate and range in particle mobilities, reducing the nominal resolution reduces the required sheath flow and hence reduces the physical size of the DMA. In turn, this reduction in physical size at the same aerosol flow rate reduces the residence time within the classification region, enabling faster scans. Additionally, for the same aerosol flow, the wider mobility window increases the particle count rate, thereby improving measurement statistics. While some applications may require higher resolution, this study demonstrates the efficacy of lower resolution measurements for ambient aerosol characterization, and illustrates the commensurate advantages of faster measurements in a smaller package.

Author contributions. SA performed the finite element modeling for the Spider DMA instrument, analyzed its measurement data, generated the figures, and wrote the manuscript text. YH analyzed the LDMA instrument data and prepared the experimental setup. BP, BCS, CMK and RXW collected the measurement data and provided technical maintenance to the instruments. JHS reviewed and provided editorial feedback on the manuscript. SVH and RCF planned the experiments, and contributed to results interpretation and editing of the manuscript.

Competing interests. RCF and SA are inventors of the "Spider" DMA technology patent (US10775290B2) which is licensed to SVH's company. The rest of the authors declare that they have no conflict of interest.

Disclaimer. Neither the United States Government nor any agency thereof, nor any of their employees, makes any warranty, express or implied, or assumes any legal liability or responsibility for the accuracy, completeness, or usefulness of any information, apparatus, product, or process disclosed, or represents that its use would not infringe privately owned rights. Reference herein to any specific commercial product, process, or service by trade name, trademark, manufacturer, or otherwise does not necessarily constitute or imply its endorsement, recommendation, or favoring by the United States Government or any agency thereof. The views and opinions of authors expressed herein do not necessarily state or reflect those of the United States Government or any agency thereof.

Acknowledgements. The authors gratefully acknowledge support by the U.S. Department of Energy, Office of Science, under Award Number(s) DE-SC0013152, by the Department of Health and Human Services, Centers for Disease Control and Prevention under Award OH010515

References

Amanatidis, S., Kim, C., Spielman, S. R., Lewis, G. S., Hering, S. V., and Flagan, R. C.: The Spider DMA: A miniature radial differential mobility analyzer, Aerosol Science and Technology, https://doi.org/10.1080/02786826.2019.1626974, 2020.

Amanatidis, S., Huang, Y., Pushpawela, B., Schulze, B. C., Kenseth, C. M., Ward, R. X., Seinfeld, J. H., Hering, S. V., and Flagan, R. C.: Efficacy of a portable, moderate-resolution, fast-scanning DMA for ambient aerosol size distribution measurements, https://doi.org/10.22002/D1.1896, https://data.caltech.edu/records/1896, 2021.

Boggs, P. T., Byrd, R. H., and Schnabel, R. B.: A Stable and Efficient Algorithm for Nonlinear Orthogonal Distance Regression, SIAM Journal on Scientific and Statistical Computing, 8, 1052–1078, https://doi.org/10.1137/0908085, http://epubs.siam.org/doi/10.1137/0908085, 1987.

Cleveland, W. S.: Robust Locally Weighted Regression and Smoothing Scatterplots, Journal of the American Statistical Association, 74, 829–836, https://doi.org/10.1080/01621459.1979.10481038, https://www.tandfonline.com/doi/abs/10.1080/01621459.1979.10481038, 1979.

Collins, D. R., Flagan, R. C., and Seinfeld, J. H.: Improved inversion of scanning DMA data, Aerosol Science and Technology, 36, 1–9, https://doi.org/10.1080/027868202753339032, 2002.

Collins, D. R., Cocker, D. R., Flagan, R. C., and Seinfeld, J. H.: The scanning DMA transfer function, Aerosol Science and Technology, 38, 833–850, https://doi.org/10.1080/027868290503082, 2004.

Creamean, J., de Boer, G., Telg, H., Mei, F., Dexheimer, D., Shupe, M., Solomon, A., and McComiskey, A.: Assessing the vertical structure of Arctic aerosols using tethered-balloon-borne measurements, Atmospheric Chemistry and Physics, 21, 1–34, https://doi.org/10.5194/acp-2020-989, https://acp.copernicus.org/articles/21/1737/2021/, 2020.

Fischler, M. A. and Bolles, R. C.: Random sample consensus, Communications of the ACM, 24, 381–395, https://doi.org/10.1145/358669.358692, https://dl.acm.org/doi/10.1145/358669.358692, 1981.

Flagan, R. C.: On Differential Mobility Analyzer Resolution, Aerosol Science and Technology, 30, 556–570, https://doi.org/10.1080/027868299304417, http://www.tandfonline.com/doi/abs/10.1080/027868299304417, 1999.

Fuchs, N. A.: On the stationary charge distribution on aerosol particles in a bipolar ionic atmosphere, Geofisica Pura e Applicata, 56, https://doi.org/10.1007/BF01993343, 1963.

Herenz, P., Wex, H., Henning, S., Bjerring Kristensen, T., Rubach, F., Roth, A., Borrmann, S., Bozem, H., Schulz, H., and Stratmann, F.: Measurements of aerosol and CCN properties in the Mackenzie River delta (Canadian Arctic) during spring-summer transition in May 2014, Atmospheric Chemistry and Physics, https://doi.org/10.5194/acp-18-4477-2018, 2018.

Hering, S. V., Spielman, S. R., and Lewis, G. S.: Moderated, Water-Based, Condensational Particle Growth in a Laminar Flow, Aerosol Science and Technology, 48, 401–408, https://doi.org/10.1080/02786826.2014.881460, http://www.tandfonline.com/doi/abs/10.1080/02786826.2014.881460, 2014.

Hering, S. V., Lewis, G. S., Spielman, S. R., Eiguren-Fernandez, A., Kreisberg, N. M., Kuang, C., and Attoui, M.: Detection near 1-nm with a laminar-flow, water-based condensation particle counter, Aerosol Science and Technology, 51, 354–362, https://doi.org/10.1080/02786826.2016.1262531, http://dx.doi.org/10.1080/02786826.2016.1262531, 2017.

Hering, S. V., Lewis, G. S., Spielman, S. R., and Eiguren-Fernandez, A.: A MAGIC concept for self-sustained, water-based, ultrafine particle counting, Aerosol Science and Technology, 53, 63–72, https://doi.org/10.1080/02786826.2018.1538549, https://www.tandfonline.com/doi/full/10.1080/02786826.2018.1538549, 2019.

Hoppel, W. A. and Frick, G. M.: Ion—aerosol attachment coefficients and the steady-state charge distribution on aerosols in a bipolar ion environment, Aerosol Science and Technology, 5, https://doi.org/10.1080/02786828608959073, 1986.

Huang, Y., Seinfeld, J. H., and Flagan, R. C.: Diffusional Transfer Function for the Scanning Electrical Mobility Spectrometer (SEMS), Aerosol Science and Technology, 6826, 1–24, https://doi.org/10.1080/02786826.2020.1760199, https://www.tandfonline.com/doi/full/10.1080/02786826.2020.1760199, 2020.

Mai, H., Kong, W., Seinfeld, J. H., and Flagan, R. C.: Scanning DMA Data Analysis II. Integrated DMA-CPC Instrument Response and Data Inversion, Aerosol Science and Technology, 52, 1–35, https://doi.org/10.1080/02786826.2018.1528006, https://www.tandfonline.com/doi/full/10.1080/02786826.2018.1528006, 2018.

Mamakos, A., Ntziachristos, L., and Samaras, Z.: Differential mobility analyser transfer functions in scanning mode, Journal of Aerosol Science, https://doi.org/10.1016/j.jaerosci.2007.11.005, 2008.

Mamali, D., Marinou, E., Sciare, J., Pikridas, M., Kokkalis, P., Kottas, M., Binietoglou, I., Tsekeri, A., Keleshis, C., Engelmann, R., Baars, H., Ansmann, A., Amiridis, V., Russchenberg, H., and Biskos, G.: Vertical profiles of aerosol mass concentration derived by unmanned airborne in situ and remote sensing instruments during dust events, Atmospheric Measurement Techniques, https://doi.org/10.5194/amt-11-2897-2018, 2018.

McMurry, P. H.: A review of atmospheric aerosol measurements, Atmospheric Environment, https://doi.org/10.1016/S1352-2310(99)00455-0, 2000.

Ortega, J., Snider, J. R., Smith, J. N., and Reeves, J. M.: Comparison of aerosol measurement systems during the 2016 airborne ARISTO campaign, Aerosol Science and Technology, https://doi.org/10.1080/02786826.2019.1610554, 2019.

Ozon, M., Stolzenburg, D., Dada, L., Seppänen, A., and Lehtinen, K. E. J.: Aerosol formation and growth rates from chamber experiments using Kalman smoothing, Atmospheric Chemistry and Physics Discussions, 2021, 1–22, https://doi.org/10.5194/acp-2021-99, https://acp.copernicus.org/preprints/acp-2021-99/, 2021.

Russell, L. M., Flagan, R. C., and Seinfeld, J. H.: Asymmetric instrument response resulting from mixing effects in accelerated DMA-CPC measurements, Aerosol Science and Technology, 23, 491–509, https://doi.org/10.1080/02786829508965332, 1995.

Stolzenburg, M. R.: An ultrafine aerosol size distribution measuring system, Doctoral dissertation, University of Minnesota, 1988.

Wang, S. C. and Flagan, R. C.: Scanning electrical mobility spectrometer, Aerosol Science and Technology, 13, 230–240, https://doi.org/10.1080/02786829008959441, 1990.

Wiedensohler, A.: An approximation of the bipolar charge distribution for particles in the submicron size range, Journal of Aerosol Science, https://doi.org/10.1016/0021-8502(88)90278-9, 1988.

Zhang, S.-H. and Flagan, R. C.: Resolution of the radial differential mobility analyzer for ultrafine particles, Journal of Aerosol Science, 27, 1179–1200, https://doi.org/10.1016/0021-8502(96)00036-5, http://linkinghub.elsevier.com/retrieve/pii/0021850296000365https://linkinghub.elsevier.com/retrieve/pii/0021850296000365, 1996.

Zhang, S.-H., Akutsu, Y., Russell, L. M., Flagan, R. C., and Seinfeld, J. H.: Radial Differential Mobility Analyzer, Aerosol Science and Technology, 23, 357–372, https://doi.org/10.1080/02786829508965320, http://www.tandfonline.com/doi/abs/10.1080/02786829508965320, 1995.

Zheng, G., Wang, Y., Wood, R., Jensen, M. P., Kuang, C., McCoy, I. L., Matthews, A., Mei, F., Tomlinson, J. M., Shilling, J. E., Zawadowicz, M. A., Crosbie, E., Moore, R., Ziemba, L., Andreae, M. O., and Wang, J.: New particle formation in the remote marine boundary layer, Nature Communications, https://doi.org/10.1038/s41467-020-20773-1, 2021.

Reviewer #1

The authors would like to thank the reviewer for their constructive feedback on this paper. Our point-to-point response to the reviewer's comments is listed below.

The manuscript by Stavros Amanatidis et al. entitled "Efficacy of a portable, moderate-resolution, fast-scanning DMA for ambient aerosol size distribution measurements" reports an intercomparison of a novel SEMS or MPSS system consisting of the "SPIDER" DMA and a "MAGIC" CPC. The main question raised in the paper is whether this system operated a relatively low DMA resolution is able to catch the key characteristics of ambient aerosol size distributions.

The paper comprehensively evaluates the transfer function of the "Spider DMA", an also reports field measurement data showing very good agreement between the novel system and a more traditional scanning DMA system.

From this reviewer's point of view, the paper is very welcome to be published in "Aerosol Measurement Techniques" although it should not be accepted for publications until following remarks have been considers in a revised version of the manuscript:

1) P1/L18ff

The authors state that traditional mobility analyzers are large and most often not suitable for UAV, but that the "Spider DMA" would be appropriate to be used on moving platforms.

It would be helpful if the authors could also elaborate on how the sheath air flow supply of the Spider DMA would look like when used on n UAV or other moving platform – especially when compared to "traditional" sheath flow supplies.

Indeed, the low flow requirements of the Spider DMA enable the usage of more compact and low-power pumps. While there are more than one options that would be appropriate for the Spider sheath flow, we included in the "Methods/Experimental" sub-section a brief description of the pump used in this prototype system, which is an in-house prototype pump based on a low-power piezoelectric micro-blower. The pump assembly weight is ~ 60 g.

2) P3/L74 ff.

The authors report the use of a soft X-ray charge conditioner. It would beneficial to specify brand / make of the specific instrument. It is not the objective of this paper, but nowadays soft x- ray ionizers are often used for size distribution measurement, without knowing the actual charging probabilities or knowing if the Fuchs charging theory is applicable without any adaptions. Therefore, at least the type of the used instrument should be stated.

We used a prototype soft X-ray charge conditioner that was developed recently at Caltech. It is based upon a Hamamatsu soft X-ray source. Detailed calibration of the charger was stopped by the COVID-19 shutdown, and further delayed when the Spider DMA was deployed to make the measurements reported in this paper. Details of the charger design and a full calibration will be reported in a separate paper. As noted by Steiner and Reischl

(2012), and Leppä et al. (2017), the charge distribution depends upon trace gases in the aerosol sample and may differ from the results of those earlier simulations. We agree with the reviewer that this is critical information for electrical mobility measurements of particle size distributions, but, since both instruments sampled the aerosol from the same charge conditioner, the conclusions drawn from the comparison presented in this paper are not affected. This note was included in Section 2.5 of the revised manuscript.

3) P5/L107:

It should be named “Fuchs charge distribution”

We revised this paragraph to the following:

“The Wiedensohler (1988) fit to the Hoppel and Frick (1986) numerical evaluation of the Fuchs (1963) charge distribution has been used in the data inversion. Note that, since both instruments sampled from the same soft X-ray charge conditioner, any deviations from the assumed charge distribution will not affect the comparison between the two instruments.”

4) P5/L114 ff

The fact that down-scan peaks have a higher maximum number ratio and are also narrower than the up-scan peaks confuses me. Typically, one would expect the opposite, where the down-scan transfer function also often exhibits a distortion or tail. Therefore, the – as far as this reviewer can say – the most common way would be to use the up-scan data for scanning DMA data rather than the down-scan data.

It would be extremely important for a clear understanding – especially for non-DMA expert readers - to elaborate in more detail on this topic and explain the differences between the down-scan/up-scan transfer functions of the Spider DMA vs. traditional DMAs.

Downscan data are often discarded from scanning DMA analyses because the shape of the transfer function is skewed, and hence more difficult to parameterize. This is true for both cylindrical and radial DMAs. However, the extent of smearing depends on how “fast” or “slow” the scan is relative to the gas mean residence time in the classifier. Collins et al. (2004) and Mamakos et al. (2008) demonstrated the shape of upscan vs downscan transfer functions, for a range of conditions for the cylindrical DMA geometry. Moderate downscan rates result in relatively small distortion in the transfer function, which is also true for the Spider DMA. In those cases, the downscan data are certainly usable. Including the downscan data improves the time resolution in scanning DMAs, which is important for some applications such as moving platform deployments.

We discuss the above in more detail in the revised paper (Section 3.1). Moreover, we included a new subsection (2.5) under “Methods” that provides some background on the scanning conditions of the two instruments used in this work.

Reviewer #2

The authors would like to thank the reviewer for their constructive feedback on this paper. Our point-to-point response to the reviewer's comments is listed below.

The authors present the application of the "Spider"-DMA to ambient measurements, demonstrating that despite the lower resolution compared to typical SMPS/DMPS systems, the characteristics of the size-distribution can be retrieved with high accuracy making the "Spider"-DMA a suitable instrument for lightweight particle size-distribution measurements. The article is written in a concise style, the presented Figures are of high quality and the conclusions are scientifically sound. The topic is certainly of interest for the community, as the interest in e.g. unmanned aerial vehicle measurements is increasing due to the usage of drones, where this device could come in handy. I can recommend publication in Atmos. Meas. Techn. subject to some minor revisions:

- 2, l.26-28: Doesn't this also come with the benefit of requiring smaller sheath-flow supplies?

This is correct; we have included a short discussion in the revised Introduction.

- 3, l.80: Standard SMPS systems often use particle counters with 1 lpm flow rate. This would increase the counting statistics compared to the spider DMA. Does the reduced resolution still outweigh the benefit of an increased sample flow in terms of counting statistics?

Considering a DMA with given geometric characteristics, the counting rate of the downstream CPC should be proportional to the ratio of aerosol flowrate-to-sizing resolution (Q_a / R). Thus, 10 / 1 lpm sheath / aerosol flow conditions (R=10) would be equivalent to 0.9 / 0.3 lpm conditions (R=3) in terms of counting statistics (both have Q_a / R = 0.1).

- 3, l.84: Why is a different sampling rate used for the LDMA system and the Spider system?

Different sampling rates were employed due to different scan durations in the two DMA systems. In both cases the sampling rate was sufficient to capture the raw counts variation during the scan.

- 4, l.90: Please be more specific on the inversion algorithm. Tikhonov regularization? What was the choice for regularization parameter? Was the same method applied to the LDMA?

We have used Tikhonov regularization for both instruments. Additional details on the data inversion are included in the revised manuscript (Section 2.5).

- 5, l.117: Please be more specific where this difference comes from. What's the difference between downscan and upscan voltage operating mode which explains these discrepancies? Figure 4 also shows that there are slight changes in the

inverted distribution. Is this happening repeatedly? And if one scan gives more precise results, why using an up- and downscan procedure instead of one direction only?

We included a discussion in the revised manuscript (Section 3.1) on the differences involved between upscans and downscans. Regarding the inverted data, analysis of all the data collected over the testing campaign showed that upscan and downscan inverted distributions were overall consistent, with upscans yielding slightly higher (~3.5%) total particle number than downscans. The advantage in using both up- and downscan data is the resulting improvement in time resolution by eliminating the time required to return to the starting voltage of a single-direction scan. The accuracy of the inverted data depends on the accuracy of the transfer function model being employed. For moderately slow downscans, this can be realized with good accuracy.

- 6, l.129: It would be very helpful to see the same for the LDMA in order to demonstrate the higher counting statistics provided by the spider DMA. What is the advantage we gain in “counts” compared to the other device?

We added a new figure in the revised paper (Fig. 5) to demonstrate the impact of resolution on DMA counting rate.

Figure 5: Compared to the LDMA there seem to be some spikes in the reconstructed total number in the Spider DMA which do not appear in the LDMA? On the contrary, the contour plot clearly shows more scatter for the inverted LDMA size-distribution. Is this caused by the lower counting statistics (see previous comment) or by a different inversion algorithm (requiring less smoothing)?

Those differences mainly arise due to the different time resolution of the two instruments. For each LDMA scan shown in the contour plot (every 6 min), there are about 6 Spider scans reported. The “spikes” that appear in the Spider data reflect the aerosol variation at those faster scans, which were not captured completely by the lower LDMA time resolution. In fact, a closer look at the number traces shows that, for the majority of these events, there is also a corresponding “spike” in the LDMA number trace, albeit typically weaker. A 6-min moving average in the Spider data would have resulted in a more “rounded” particle number time series.

- Figure 6: Similar to the above comment, the spider size-distribution looks extremely “smooth” here. What is causing this?

The Spider distribution appears smoother because of the combined effect of two factors: a) more smoothing was added in the Spider inversion compared to the LDMA (details included in the revised manuscript – Section 2.5); b) the 30-min average distributions shown in Fig. 6 include about 6 times more Spider scans than the LDMA (i.e., 27 vs. 5 scans), which results in a “smoother” mean distribution over the same time interval.

- 11, l.185: Are the GMD and total number the only key characteristics of a size-distribution? I would be a bit more defensive with that statement.

We have revised our statement to the following:

"The present results suggest that two key characteristics of ambient size distributions, geometric mean diameter and number concentration, are sufficiently captured when operating the DMA at lower resolution than is typically employed."

- 11, l.185: Related to the fact that lower resolution is perfectly suitable in reconstructing aerosol formation and growth rates there is a recent paper in Atmos. Chem. Phys. Discuss. by Ozon et al. (https://doi.org/10.5194/acp-2021-99), showing that a wider resolution can indeed help to reconstruct aerosol dynamics process rates. Even if it is at preprint stage, it could be mentioned here as it is making a similar case that size-distribution reconstruction in ambient or chamber experiments does not necessarily require high resolution.

We thank the reviewer for the suggestion; we have added the reference in the Introduction of the revised paper.

Reviewer #3

The authors would like to thank the reviewer for their constructive feedback on this paper. Our point-to-point response to the reviewer's comments is listed below.

The authors provide a concise and well reasoned analysis of a relatively low resolution spider DMA system as a means to balance classifier size and robustness of data capture. The analysis of the transfer functions were performed by steady state laminar CFD analysis, which is appropriate for this system (done in separate study). The modeled results are in line with findings from other studies and give a quantified potential for weight and resolution tradeoffs. As a whole the article is worth of publication and should be accepted once addressing the following comments.

My largest disappointment in the article is that it did not engage more broadly with the larger question of what are the theoretical and practical tradeoffs that allow classifiers (in this case DMAs) to be optimized for specific applications. This work gives one data point as to a classifier that works well for the desired application, but does not give the reader insights into whether the system could be further optimized by tradeoffs. A particularly useful inclusion would be general scaling laws that might guide others in the field who are seeking to develop custom classifiers for small (either volume or mass limited) applications.

We agree with the reviewer that this is an important question that needs to be addressed in more detail. This present paper, however, focuses on reporting the efficacy of the moderate-resolution Spider DMA in measuring ambient size distributions, rather than the process of DMA design & optimization, which was (in part) presented in a previous

publication (Amanatidis et al, 2020). Thus, even though this is indeed a topic of interest for the authors, it is outside of the scope of this present work.

Minor points for the article are as follows:

Line 55: Despite the work being based on a previous publication (Amanatidis, 2020) it would be useful to have a schematic in Sec 2.2 to depict basic model parameters and methodology, such as labeled boundary conditions and a few rudimentary results.

We have included additional details on the finite element modeling in the supplementary material, including a schematic of the Spider geometry used in the modeling (Figure S1), as well as a figure with particle trajectories over the voltage scan (Figure S2).

Line 68: It was unclear why the intervals for injection were chosen and what impact it had on the simulation results.

Shorter injection interval (i.e., larger number of particles simulated over the scan) was employed for smaller particles to capture in sufficient detail the additional (Brownian) motion along the trajectories of those diffusive particles.

Line 107: Why was Wiedensohler approximation chosen for an x-ray charger when the ion properties of soft x-ray have been shown to be different than Wiedensohler's results which are calibrated to radioactive neutralizers?

We agree with the reviewer that the Wiedensohler approximation employed might differ from the actual charge probability generated by the soft X-ray charge conditioner. The device used here was a prototype charge conditioner that was developed recently at Caltech, but has not yet been fully characterized. We employed the Wiedensohler correlation as an approximation to the actual charge distribution. Since both instruments sampled the aerosol from the same charge conditioner, the conclusions drawn from the comparison presented in this paper are not affected.

Line 116: It would be nice to have the maximum number ration and "narrower" transfer functions discussed in quantified terms.

We present a comparison between the parameters of the upscan and downscan transfer functions in the supplementary material, Figure S3.

Fig. 3b: I like the visual representation of the scans in Fig 3b, but a quantitative figure would also be useful depicting higth and width of the transfer function.

Figure S3 in the supplementary material presents a more quantitative comparison between the height, width, and area of the upscan and downscan transfer functions.

Line 130: how are the smooth lines fit to the data? What are the smoothing parameters?

We included additional details on the smoothing employed to the raw counts data in the revised manuscript (Section 2.5).

Fig. 6: The smaller modes of the distributions appear to be less distinct in the right plots making them indistinguishable. I would appreciate the authors view of these findings.

Due to the variability of the size distribution over this transient event, and the different time resolution of the two instruments, it is not straightforward to make a conclusive comparison that would explain such subtle differences. We have, however, investigated whether the low resolution of the Spider DMA could potentially be a limitation in capturing bimodal distributions similar to those shown in Figure 6; based on our preliminary analysis, this was not the case. This is also supported by observing the shaded light blue area in panel b, that represents the variability of the size distribution over the averaging interval, which shows that the Spider data included scans where the 1st mode of the distribution was distinguishable.

Typesetting – the authors provide correct spacing between the number and engineering unit, e.g. L/min, in most cases, but fail to provide spaces between numbers and seconds or volts in several places.

Corrected in the revised manuscript.